JACS
JOURNAL OF THE AMERICAN CHEMICAL SOCIETY

Article

pubs.acs.org/JACS

Evidence for a Di-μ-oxo Diamond Core in the Mn(IV)/Fe(IV) Activation Intermediate of Ribonucleotide Reductase from *Chlamydia trachomatis*

Ryan J. Martinie,[†] Elizabeth J. Blaesi,[†] Carsten Krebs,[†,‡] J. Martin Bollinger, Jr.,[†,‡] Alexey Silakov,*[,†] and Christopher J. Pollock*[,†]

[†]Department of Chemistry and [‡]Department of Biochemistry and Molecular Biology, The Pennsylvania State University, University Park, Pennsylvania 16802, United States

Supporting Information

ABSTRACT: High-valent iron and manganese complexes effect some of the most challenging biochemical reactions known, including hydrocarbon and water oxidations associated with the global carbon cycle and oxygenic photosynthesis, respectively. Their extreme reactivity presents an impediment to structural characterization, but their biological importance and potential chemical utility have, nevertheless, motivated extensive efforts toward that end. Several such intermediates accumulate during activation of class I ribonucleotide reductase (RNR) β subunits, which self-assemble dimetal cofactors with stable one-electron oxidants that serve to initiate the enzyme's free-radical mechanism. In the class I-c β subunit from *Chlamydia trachomatis*, a heterodinuclear Mn(II)/Fe(II) complex reacts with dioxygen to form a Mn(IV)/Fe(IV) intermediate, which undergoes reduction of the iron site to produce the active Mn(IV)/Fe(III) cofactor. Herein, we assess the structure of the Mn(IV)/Fe(IV) activation intermediate using Fe- and Mn-edge extended X-ray absorption fine structure (EXAFS) analysis and multifrequency pulse electron paramagnetic resonance (EPR) spectroscopy. The EXAFS results reveal a metal−metal vector of 2.74−2.75 Å and an intense light-atom (C/N/O) scattering interaction 1.8 Å from the Fe. Pulse EPR data reveal an exchangeable deuterium hyperfine coupling of strength |T| = 0.7 MHz, but no stronger couplings. The results suggest that the intermediate possesses a di-μ-oxo diamond core structure with a terminal hydroxide ligand to the Mn(IV).

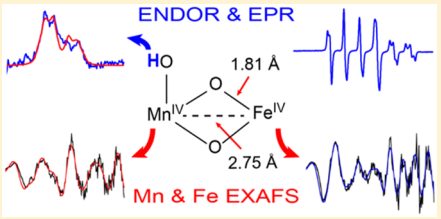

INTRODUCTION

Metalloenzymes catalyze a diverse array of biochemical reactions in metabolism and regulation; some of the most chemically challenging of these reactions are effected by high-valent iron and manganese complexes. Among a myriad of other examples,[1−7] the oxidation of methane to methanol by the soluble form of methane monooxygenase (sMMO),[8−11] the production of deoxyribonucleotides for DNA synthesis and repair,[12−15] water oxidation by the oxygen evolving complex of photosystem II,[16−18] and metabolism of the majority of prodrugs in humans[19,20] all involve such complexes at key steps. A robust understanding of the structures of these potent intermediates and how enzymes generate and control them is central to efforts to develop bioinspired catalysts for water oxidation, C−H-bond activation, and other processes not yet mastered by synthetic chemists.[7,21]

The ferritin-like dimetal-carboxylate (FDC) oxidases and oxygenases are a particularly illustrative example of how structurally similar proteins can direct different pathways for formation and decay of high-valent transition metal intermediates and thereby specify different outcomes. Members of this important enzyme superfamily utilize a largely conserved protein structure and ligand sphere to bind nonheme dimetal cofactors that interact with dioxygen or reduced forms thereof to generate an array of distinct intermediates and carry out diverse biological functions.[22] One of the most extensively studied FDC proteins, the hydroxylase component of soluble methane monooxygenase (sMMOH), effects the conversion of methane to methanol. sMMOH activates oxygen at its diiron(II/II) cluster to form a μ-peroxodiiron(III/III) complex, P (or H_{peroxo}), which subsequently decays to the high-valent intermediate, Q, a diiron(IV/IV) complex.[9,23] The potently oxidizing Q overcomes the high homolytic C−H bond-dissociation energy (104 kcal/mol) of methane to initiate its hydroxylation. An analogous mechanism has been proposed for the related fatty acid desaturases.[24] Another FDC protein, aldehyde deformylating oxygenase (ADO), converts C_n fatty aldehydes to the corresponding C_{n-1} alk(a/e)nes and formate, a formally redox-neutral conversion.[25−27] ADO activates oxygen, purportedly via a diiron(III/III)-peroxyhemiacetal complex,[28,29] which undergoes univalent reduction to initiate a radical-scission reaction that cleaves the C−C bond.[29] Thus, different members of the FDC family utilize divergent mechanistic strategies to achieve chemically diverse outcomes.

Additional distinct outcomes occur in the β subunits of class I ribonucleotide reductases (RNRs). RNRs catalyze the reduction of ribonucleotides to deoxyribonucleotides via a

Received: November 7, 2016
Published: January 11, 2017

DOI: 10.1021/jacs.6b11563
J. Am. Chem. Soc. 2017, 139, 1950−1957

largely conserved free-radical mechanism,[13,30] initiated by a transient cysteine-thiyl radical.[31,32] In class I RNRs, present in eukaryotes as well as some bacteria and archaea, this thiyl radical is generated by a long-range electron transfer from the cysteine in the α subunit to a stable, one-electron oxidant in the β subunit.[31,33] The β subunit is an FDC protein, and the dimetal cofactor serves either directly as the catalytically required oxidant or to generate this oxidant. In a class I-a RNR, the diiron(II/II) form of the β subunit reacts with oxygen to form a μ-peroxodiiron(III/III) complex akin to P in sMMOH,[34−36] but instead of undergoing a redox-neutral conversion to a Q-like diiron(IV/IV) complex, it (or its nonaccumulating successor) instead undergoes one-electron reduction to produce the diiron(III/IV) complex, X.[12,37] X oxidizes a nearby tyrosine to form a stable tyrosyl radical cofactor,[38−42] which serves as the initiating one-electron oxidant of the cysteine in α. Class I-b enzymes employ a structurally similar dimanganese cluster to install the tyrosyl radical;[43−45] rather than reacting directly with dioxygen, the dimanganese(II/II) cofactor reacts with superoxide (generated from O_2 by a flavin-containing activator protein, NrdI, that forms a complex with the RNR β subunit) to form a dimanganese(III/IV) intermediate that oxidizes the tyrosine.[15,43,46] In contrast, the β subunits of class I-c RNRs, exemplified by the protein from *Chlamydia trachomatis* (*Ct*), have a phenylalanine at the sequence position occupied by the radical-harboring tyrosine in the class I-a/b subunits.[47] The stable one-electron oxidant is instead harbored directly on the metallocofactor, a Mn(IV)/Fe(III) complex.[14,48−51] In the *Ct* RNR β subunit, the Mn(II)/Fe(II) complex reacts with dioxygen to generate a Mn(IV)/Fe(IV) intermediate (hereafter denoted **4**/**4**; Scheme 1),[52] which is reduced by one electron to form the active Mn(IV)/Fe(III) cofactor.[53]

Scheme 1. Activation Pathway of the Class I-c Ribonucleotide Reductase[a]

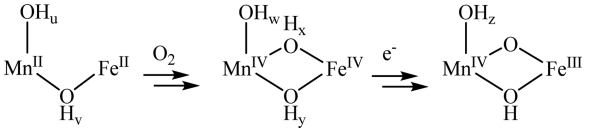

[a]Subscripted letters u−z are intended to designate protonation states that are not known; each term thus has an integer value ranging from 0 to 2.[51,52,54]

The FDC proteins thus constitute a remarkably flexible scaffold that can use iron or manganese in diverse O_2-activation chemistry that enables multiple essential biological functions. This functional flexibility depends on the capacity of the individual proteins to direct formation of intermediate states with appropriate reactivity, to avoid formation of alternative high-valent complexes, and, thereby, to suppress undesired outcomes (e.g., self-hydroxylations) for which the FDC scaffold is competent. To understand the structural basis for this control of reaction pathway, it is necessary to define the manifold of structures represented among these high-valent intermediates. Historically, structural characterization of these complexes has been fraught with controversy. Indeed, despite the more than two decades of scrutiny, Q and X continue to be subjects of structural studies. Nearly 20 years ago, an examination of Q by extended X-ray absorption fine structure (EXAFS) suggested an Fe−Fe distance of only 2.46 Å, leading to the proposal of a di-μ-oxo diamond core structure for the intermediate.[10] However, for the ensuing 19 years, this structural assignment has remained controversial, as such a short distance could not readily be reproduced in either computational models or small molecule mimics,[55−58] and other studies suggested that an "open core" might, in fact, be significantly more reactive for the H·-abstraction step needed to initiate methane hydroxylation.[55] More recent continuous-flow resonance Raman experiments were interpreted in favor of the originally proposed diamond-core geometry,[11] but it remains unclear whether a structure with a 2.46 Å Fe−Fe separation is possible. Similar controversy has surrounded the structure of X. An early EXAFS study concluded that it also has an unusually short Fe−Fe distance of only 2.5 Å,[59] but a more recent study on more concentrated samples gave an Fe−Fe distance of 2.8 Å,[60] compatible with the distance expected of a di-μ-oxo core. Potentially at odds with the conclusions of the second EXAFS study, magnetic circular dichroism (MCD) experiments were interpreted as necessitating that one of the two single-atom (presumably oxygen) bridges, required to give the short Fe−Fe distance determined by EXAFS, be protonated (i.e., a μ-oxo/μ-hydroxo core).[61,62] However, distances longer than the measured 2.8 Å are predicted for such a core,[60] and electron nuclear double resonance (ENDOR) experiments on X carried out over 20 years have consistently shown no evidence for the required proton of a hydroxo bridge.[37,63−65] Compounding the uncertainty, the most recent ENDOR work suggested that it might have only a single nonprotein oxygen bridge, a conclusion that is potentially incompatible with the short Fe−Fe distance.[66] Clearly, whereas the structures of these intermediates are of significant interest, the history of attempts to define them has been rife with controversy.

The Mn(IV)/Fe(IV) activation intermediate in the class I-c RNR β subunit (**4**/**4**) is directly analogous to sMMOH Q_t in that both metals have a formally +IV oxidation state following direct reaction of the dimetal(II/II) cluster with dioxygen. On this basis, it was suggested that **4**/**4** might also have a di-μ-oxo diamond core geometry,[52] although no dispositive evidence for or against this hypothesis has been reported. Investigation of the structure of **4**/**4** has the potential to illuminate mechanisms of oxygen activation at heterodinuclear Mn/Fe sites, for which the range of chemical capabilities remains underexplored relative to that of their diiron counterparts. The potential of this manifold for difficult oxidation outcomes has been underscored recently by the discovery of the "R2lox" family of proteins, in which a heterodinuclear Mn/Fe site has been shown to activate an aliphatic C−H bond and an aryl O−H bond in formation of an intraprotein Val-Tyr cross-link.[67,68] This reactivity contrasts with the one-electron chemistry performed by **4**/**4**, reminiscent of the divergent functions of the diiron complexes, Q and X. Moreover, **4**/**4** remains, to our knowledge, the only known example of a Mn(IV)/Fe(IV) complex, and its structure is therefore of fundamental interest in inorganic chemistry.

The heterodinuclear nature of **4**/**4** confers a number of distinct advantages in investigating its structure. First, it leads to a ground state with total electron spin, S_{tot}, of 1/2 (by contrast to the integer-spin ground state of Q), enabling application of electron paramagnetic resonance (EPR) methods.[52] Second, it allows the structure of the cofactor to be probed in site-selective fashion by X-ray absorption spectroscopy (XAS), as was previously done for the active Mn(IV)/Fe(III) state.[54] A third advantage, conferred by the size and solubility of the *Ct*

DOI: 10.1021/jacs.6b11563
J. Am. Chem. Soc. 2017, 139, 1950−1957

RNR β subunit and the favorable formation and decay kinetics of the intermediate, is that **4**/**4** can be prepared in relatively high concentration and purity,[52] a factor that has proven relevant in the structural investigation of X.[60] Capitalizing on these advantages, we interrogated **4**/**4** by a combination of XAS and EPR spectroscopy to deduce the structure of its inorganic core.

RESULTS AND DISCUSSION

Samples containing high concentrations of **4**/**4** were prepared by using the previously reported method of *in situ* generation of oxygen from chlorite with the enzyme chlorite dismutase (for details, see the Supporting Information).[69] Because EXAFS probes all absorbers in a sample, knowledge of the sample composition was critical for proper data analysis; detailed speciation information was obtained by analysis of the Mössbauer spectra of the samples ([Fe] = 2.6 mM; [Mn] = 2.6 mM; 65% **4**/**4**; for details, see the Supporting Information).[52,69]

The Fe *K*-edge EXAFS data and fits (Figure 1 top and Table 1) reveal a first coordination sphere composed of a shell of

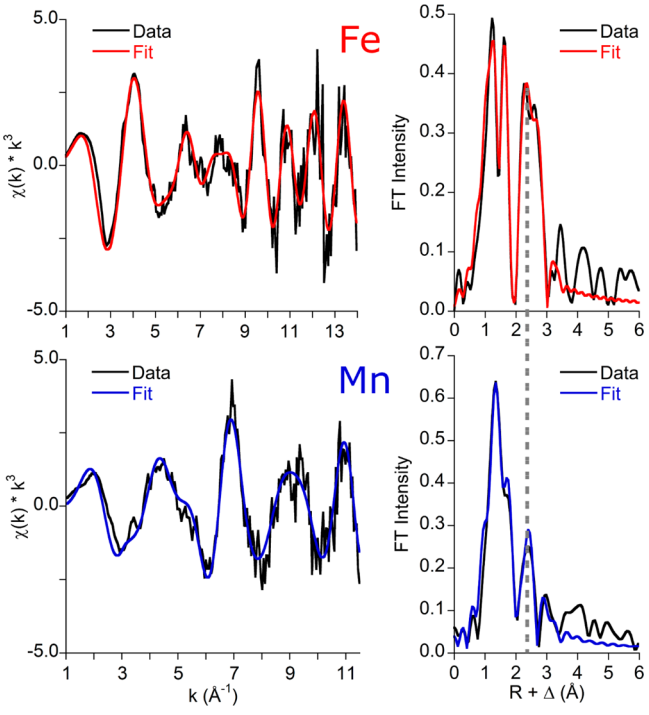

Figure 1. EXAFS traces (left) and corresponding Fourier transformed data (right) of **4**/**4**-containing samples at the iron (top) and manganese (bottom) edges. Experimental traces are black, and fits using parameters presented in Table 1 are red (Fe) and blue (Mn). A putative metal−metal interaction (dashed line) is observed in both Fourier transforms at ∼2.75 Å. Experimental data were acquired and fit for k = 1−14 Å^{-1} for Fe and 1−11.5 Å^{-1} for Mn.

light-atom scatterers at an average distance of 1.81 Å and another shell at an average of 2.01 Å. Both fit best with a coordination number of two. At longer distances, an Fe−Mn interaction is seen at 2.74 Å, and light-atom scatterers are observed at 2.97 and 3.33 Å. A contribution at 2.5 Å is also present, reminiscent of the early EXAFS data on Q and X, but this intensity could not be acceptably fit with a metal scatterer (see tables in the Supporting Information).

The Mn *K*-edge EXAFS data and fits (Figure 1 bottom and Table 1) provide a picture that is complementary to that afforded by the Fe data. A first shell of scatterers can be fit at a distance of 1.86 Å. This distance, significantly less than the ∼2.0 Å expected for protein-derived ligands to Mn(IV), suggests that the first shell is made up of both protein ligands and nonprotein oxygen (e.g., oxo or hydroxo) ligands at an *average* distance of 1.86 Å from the Mn(IV). The lack of resolution of protein and nonprotein constituents of this first shell can be rationalized by the lower resolution in the Mn EXAFS data (∼0.15 Å), which results from the limited k-range that can be interrogated before the Fe edge interferes (at k = 12). A smaller contribution at 2.19 Å, likely a result of the ∼30% Mn(II) contaminant in the sample, is also present. As with the fits to the Fe K-edge data, a metal scatterer is observed at 2.75 Å, and metal-light atom interactions are seen at longer distances. These distances are quantitatively consistent with those obtained in a density functional theory (DFT) optimized model for **4**/**4** with a di-μ-oxo core.[58] Importantly, no interaction is observed at 2.5 Å, confirming that the intensity observed at that distance in the Fe data does not arise from a metal scatterer. For both metal edges, the sum of the coordination numbers for the first coordination spheres is less than the expected value of six. We attribute this discrepancy to static disorder within the samples, which coalesces multiple shells of scatterers in a manner that cannot adequately be modeled by the assumption of a Gaussian distribution of distances embodied by the Debye−Waller parameter.[70] Similar observations have been noted in previous studies on high-valent dimetal complexes.[10,71]

These EXAFS data provide structural metrics that drastically limit the range of possible core structures for **4**/**4**. The first coordination sphere of the Fe contains two shells: one at 1.81 Å and the other at 2.01 Å. The latter is consistent with the expected distances between Fe(IV) and protein ligands. The 1.81 Å distance is too short for protein (∼2.0 Å) or hydroxide ligands (1.85−1.95 Å) and too long for a terminal oxo (∼1.65−1.70 Å), but it is entirely consistent the distance expected for a bridging oxo ligand (∼1.80 Å).[55,72,73] Although the observed number of scatterers in the best fit to the data (two) is not a reliable quantitative measure, the intensity of this feature in the FT is notably high, particularly by comparison to those for complexes known to have a single oxo scatterer. Moreover, the intensity of this feature is very similar to that reported for a di-μ-oxo-diiron(IV) diamond core complex; in fact, the entire Fourier transform for the Fe-edge in the data for **4**/**4** is similar to that for the diiron(IV) complex.[55] Because the iron in its binding site should have only two open coordination sites,[74−76] the presence of two oxo scatterers would preclude the presence of a μ-hydroxo ligand; the analysis would therefore suggest that **4**/**4** could have a di-μ-oxo diamond core geometry.

The metal−metal (M-M) scattering interaction at 2.74−2.75 Å, observed in both the Mn and Fe edge data, is markedly short. While no structurally characterized high-valent Mn−Fe model compounds that might serve as direct precedents have been reported, Mn(IV)/Mn(IV),[71,77−79] Fe(IV)/Fe(IV),[55,73] and Fe(IV)/Fe(III)[72,80] models are known. Among those complexes with two oxo bridges, the range of M−M distances is 2.67−2.78 Å. By contrast, the known inorganic complexes with one oxo and one hydroxo bridge have M-M distances in the range of 2.79−2.91 Å, and a di-μ-hydroxo complex has a M−M distance of ∼2.93 Å (Figures S1 and S2). The observed distance of 2.74−2.75 Å for **4**/**4** is thus uniquely consistent with those of the di-μ-oxo-dimetal models. This distance also

DOI: 10.1021/jacs.6b11563
J. Am. Chem. Soc. 2017, 139, 1950−1957

Table 1. Numerical Results from Fits to the Fe and Mn EXAFS[a]

Fe				Mn			
scatterer	N	R (Å)	σ^2 (Å^2)	scatterer	N	R (Å)	σ^2 (Å^2)
Fe−C/N/O	2	1.81	0.00978	Mn−C/N/O	2	1.86	0.00722
Fe−C/N/O	2	2.01	0.00636	Mn−C/N/O	1	2.19	0.00422
Fe−C/N/O	2	2.50	0.00400	Mn−Fe	0.7	2.75	0.00472
Fe−Mn	1	2.74	0.00384	Mn−C/N/O	2	2.99	0.00315
Fe−C/N/O	4	2.97	0.00542	Mn−C/N/O	2	3.28	0.00620
Fe−C/N/O	1	3.33	0.00271				
F		0.467		F		0.401	
E_0		−2.05 eV		E_0		2.77 eV	

[a]Uncertainty in distance determinations are ±0.02 Å.

precludes monobridged, "open-core" structures, which exhibit even longer M-M distances (~3.4 Å).[73] Such structures would also not be expected to yield the unusually intense 1.81-Å interaction observed in the Fe EXAFS (vide supra), because a single μ-oxo would be expected at ~1.8 Å, and an additional terminally coordinated oxo (if present), would be closer to the metal ion (1.65−1.70 Å), likely unresolved, and therefore anticipated to shift the peak arising from the μ-oxo to a value less than 1.8 Å.

Although high-valent heterodinuclear models are unavailable, the Mn(IV)/Fe(III) form of *Ct* RNR β offers a valuable point of comparison. On the basis of EXAFS analysis, this form of the cofactor was assigned as having a μ-oxo/μ-hydroxo diamond core structure;[54] this conclusion was corroborated by results from nuclear resonance vibrational spectroscopy (NRVS) and MCD spectroscopy.[81] The EXAFS investigation indicated a Mn−Fe distance of 2.92 Å, ~0.17 Å longer than the distance observed for **4**/**4** (vide supra). This elongation would be expected to occur following one-electron reduction of the iron site and protonation of one of the oxo bridges.[71]

The conclusion that the two presumptive bridging oxygen ligands are unprotonated emerges only indirectly from the EXAFS data, on the basis of comparisons of measured distances to those found in a limited set of well-characterized homodinuclear model complexes. Moreover, the data provide no information concerning the protonation state of the expected terminal oxygen ligand to the Mn(IV) site (Scheme 1), due in part to the low resolution of the Mn EXAFS data. In order to address these questions, we examined **4**/**4** by multifrequency pulse EPR techniques. In **4**/**4**, the Mn(IV) has an electron-spin quantum number, S, of 3/2 and couples antiferromagnetically to the Fe(IV) ion (S = 2), resulting in an overall S_{tot} = 1/2 ground state, which makes the complex amenable to EPR characterization.[52] The continuous-wave (CW) X-band spectrum of **4**/**4** reflects strong hyperfine (HF) coupling of the unpaired electron with the ^{55}Mn nucleus (with nuclear-spin quantum number, I, of 5/2), which splits the resonance into six discrete packets (Figure 2A). Using simultaneous, multifrequency simulation, both X- and Q-band spectra can be simulated with parameters g = [2.028, 2.021, 2.013] ± 0.001 and A_{Mn} = [221, 243, 246] ± 5 MHz, in reasonable agreement with previously published parameters (Figure S3).[52] EPR can afford useful structural information by revealing HF couplings to nearby magnetic nuclei, including hydrons that are invisible to EXAFS analysis. In particular, observation of HF couplings to exchangeable hydrons might reveal the ligand protonation states and provide a more direct assessment of the nature of the bridging and terminal nonprotein oxygen ligands. To probe exchangeable hydrons,

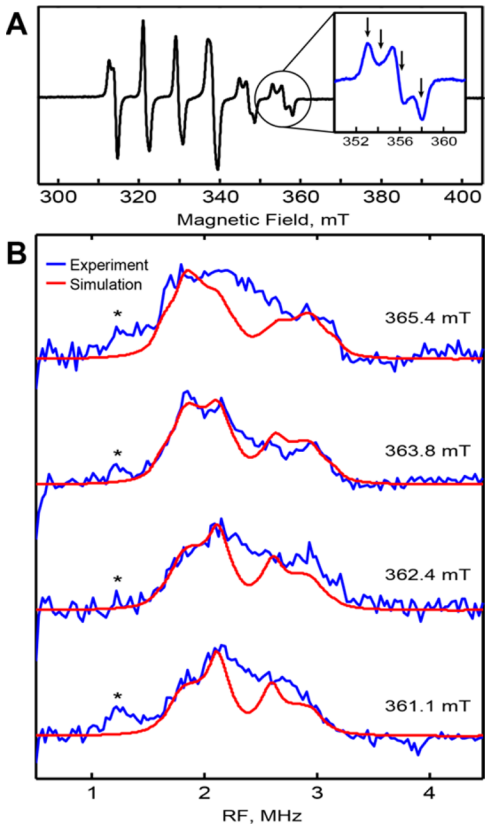

Figure 2. Interrogation of **4**/**4** by electron paramagnetic resonance methods. (A) Continuous-wave, X-band spectrum with expanded view of the packet at the highest magnetic field (inset). (B) X-band, field-dependent, ^{2}H-ENDOR spectra (blue) and simulations (red) of **4**/**4** prepared in D_2O. The field positions for the ENDOR spectra are indicated by the arrows in the inset of panel (A) . The peaks marked with an asterisk are artifacts due to experimental setup. The deviations between the experimental and simulated spectra near the Larmor frequency (ν_L = 2.36, 2.37, 2.38, and 2.39 MHz at 361.1, 362.4, 363.8, and 365.4 mT, respectively) are attributable to matrix deuterons. All measurements were performed at 15 K. CW and ENDOR measurements were performed with microwave frequencies of 9.628 and 9.702 GHz, respectively.

field-dependent deuterium electron−nuclear double resonance (^{2}H-ENDOR) spectra were recorded at X-band on a sample of **4**/**4** prepared in ^2H_2O (D_2O) buffer (Figure 2B). Comparison to spectra recorded under identical conditions on a sample prepared in H_2O buffer indicates that the observed signals are attributable to deuterium and that there is no observable interference from other nuclei (e.g., ^{14}N) in this frequency

DOI: 10.1021/jacs.6b11563
J. Am. Chem. Soc. 2017, 139, 1950−1957

regime (Figure S4). The ^{2}H-ENDOR spectra can be simulated with a single predominantly anisotropic hyperfine coupling (Figure 2B) A_{2H} = [-0.90, −0.43, 1.41] ± 0.1 MHz with Euler angles [0, 25, 0] ± 15° (see the Supporting Information for additional details). The deuterium nuclear quadrupole interaction was simulated with the tensor [-0.07, −0.07, 0.14] ± 0.03 MHz and Euler angles [0, 110, 0] ± 20°.

To verify the absence of stronger couplings (which might, in theory, be obscured by the periodic blindspots inherent in the Mims ENDOR pulse sequence utilized above), we performed additional X- and Q-band ENDOR measurements of the ^{1}H region (Figure S5). The overall breadth of the field-dependent ^{1}H-ENDOR spectra are compatible with the ^{2}H hyperfine coupling detailed above; no stronger couplings were observed.

The magnitude of the observed anisotropic HF coupling (|T| = 0.7 MHz) and the rhombicity parameter (ε = 0.3), extracted from the observed ^{2}H HF coupling, can be related to geometric information via a model that accounts for dipolar coupling of the deuterium nucleus to the S = 3/2 Mn(IV) center and the S = 2 Fe(IV) center, weighted according to their spin-projection factors (Figure S6; for details, see Supporting Information). HF parameters calculated according to this model for ^{2}H nuclei located at different positions relative to the Mn(IV)/Fe(IV) cluster were compared to the measured values. The resulting compatible positions are shaded black in Figure 3, with lighter shading indicating less good agreement; the shaded region constitutes a "geometric confidence interval."

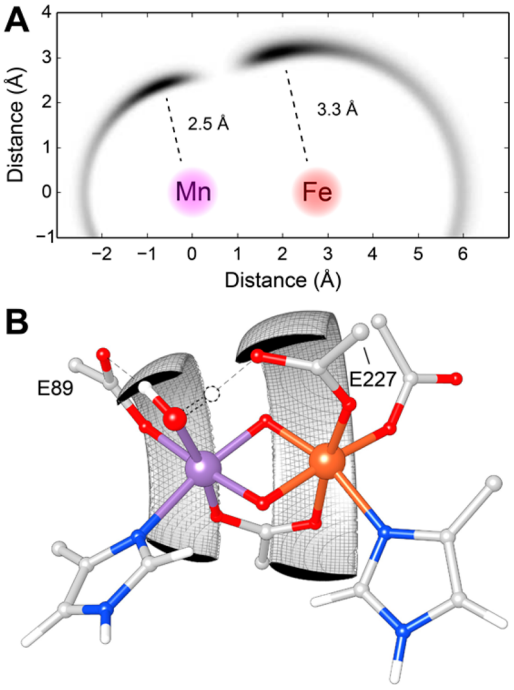

Figure 3. Assessment of the geometric disposition of the detected exchangeable deuterium in **4**/**4** with respect to the Mn(IV)/Fe(IV) cluster. (A) Positions compatible with the observed ^{2}H-hyperfine coupling (black shading), relative to the Mn−Fe. The plane of the paper represents an arbitrary plane containing Fe, Mn, and the deuteron of interest. (B) Compatible positions (isosurface at 50% of the maximum according to eq S4) represented in three dimensions, superimposed on a three-dimensional model of **4**/**4**, based on data from Noodleman and co-workers.[58] Atoms are color-coded as follows: manganese (magenta), iron (rust), carbon (gray), nitrogen (blue), oxygen (red), and hydrogen (white).

The resulting metal-^{2}H distances are most compatible with a terminal hydroxide/water ligand to the Mn(IV). The analysis gives two mathematically compatible regions: one ∼2.45 Å from Mn and the other ∼3.25 Å from Fe (Figure 3A). In both cases, the observed coupling is too strong to be compatible with exchangeable hydrons on first- and second-sphere residues (e.g., coordinating histidines), as the closest exchangeable hydrons are expected to be >5.0 Å from both the Mn site and the Fe site, giving rise to couplings with magnitude less than or equal to 0.1 MHz.[58,74−76] Furthermore, the observed coupling is both too weak and insufficiently rhombic to be assigned to the ^{2}H nucleus of a bridging hydroxide (|T| ∼ 1.7−2.3 MHz, ε ∼ 0.8−1.0).[65,68,82−84] The ∼2.45 Å possibility is compatible with a hydroxide/water ligand to Mn(IV), on the basis of typical bond lengths/angles (2.4 ± 0.1 Å).[54,58,78,79] In contrast, the ∼3.25-Å possibility does not correspond to any ^{2}H that could be bonded to one of the known heteroatoms in a chemically reasonable geometry, being too far away for a hydroxide/water ligand to Fe(IV).

The structural assignment of a terminally coordinated hydroxide/water ligand to Mn(IV) can be further refined by consideration of the coordination sphere and the local hydrogen bonding network (Figure 3B). The open coordination site for Mn(IV) is approximately perpendicular to the Mn−Fe vector. Moreover, the Fe−Mn−O-H dihedral angle is, theoretically and in the absence of restrictive hydrogen-bonding interaction, subject to change by free rotation about the Mn−O bond. However, the many available structures of RNR β subunits suggest that hydrogen bonding interactions to either Glu 89 or Glu 227 (or both) could very well restrict this rotation and bias or fix the dihedral angle. Thus, there are two likely positions for the exchangeable hydron, one in which the O−H bond is oriented generally toward the Fe ion, allowing the hydroxo ligand to donate an H-bond to Glu 227, and another oriented away from the Fe, allowing H-bond donation to Glu 89 (Figure 3B). Intriguingly, a deuteron oriented toward Glu 227 is expected to exhibit a coupling that is significantly more rhombic (ε = 0.8−1.0) and somewhat larger (|T| ∼ 0.8) than the observed coupling (hydrogen with dashed outline in Figure 3B). In contrast, the position oriented away from the iron is completely compatible with the observed hyperfine coupling, as the expected position (Figure 3B) shows significant overlap with the region indicated by the EPR data (black shading/isosurface). These data cannot definitively assign the observed signals as arising from a single deuteron (i.e., on a hydroxide ligand), rather than two (i.e., on a water ligand); it is possible that the observed signal arises from the superposition of two nonidentical HF couplings or from two indistinguishable HF couplings. However, we favor the hydroxide possibility because (i) a single HF coupling is sufficient to simulate the data, and (ii) a second ^{2}H nucleus would likely lie in the position hydrogen bonded to Glu 227, which would, due to the greater rhombicity predicted by the model, exhibit a significantly larger coupling in one orientation than that observed (rather than being indistinguishable).

The EXAFS and ENDOR data represent orthogonal probes of the structure of **4**/**4** and together suggest a di-μ-oxo diamond core structure with a terminally coordinated hydroxide ligand to Mn(IV) (Figure 3B). The short Mn−Fe distance (2.74−2.75 Å) observed in both Mn- and Fe-edge EXAFS data requires at least two bridging atoms and precludes monobridged or "open-core" structures. Among di-μ-(hydr)oxo diamond core structures, a di-μ-oxo is most compatible with

DOI: 10.1021/jacs.6b11563
J. Am. Chem. Soc. 2017, 139, 1950−1957

both the M−M distance (by comparison to well-characterized models) and the intense 1.81 Å first shell of scatterers around Fe. Moreover, the presence of a μ-hydroxo ligand would give rise to a large, rhombic HF coupling from an exchangable hydron, which is not present. An exchangeable hydron is observed by ^{2}H-ENDOR, with parameters consistent with a terminal hydroxide/water ligand to Mn(IV). This signal is most compatible with a terminally coordinated hydroxide ligand to Mn(IV), hydrogen bonded to Glu 89, though water cannot be explicitly ruled out on the basis of the available data. This comprehensive assignment represents the first structural characterization of any Mn(IV)/Fe(IV) complex and adds to the very few reported for other types of biological high-valent transition metal complexes.

MATERIALS AND METHODS

Preparation of 4/4 Samples for XAS and EPR Analysis. The β subunit of *Chlamydia trachomatis* (*Ct*) ribonucleotide reductase was overexpressed and purified to homogeneity as previously described.[14] Following removal of oxygen,[2] *Ct* β_2, Mn(II), Fe(II), and chlorite dismutase were mixed to final concentrations of 2.2 mM, 3.3 mM, 3.3 mM, and 25 μM, respectively.[69] This mixture was rapidly mixed in a 4:1 volume ratio with a 50 mM solution of sodium chlorite, and the reaction solution was rapidly frozen after 0.23 s in liquid ethane (XAS) or isopentane (EPR).

XAS Data Collection and Processing. X-ray absorption spectra were collected on beamline 7-3 at the Stanford Synchrotron Radiation Lightsource under ring conditions of 3 GeV and 500 mA. A Si(220) monochromator (φ = 90°) was used for energy selection of the incident beam; harmonic rejection was achieved using a Rh-coated mirror (9 keV) and by detuning the monochromator by 25%. The energy of the incident beam was calibrated using metal foils upstream of the sample (7111.3 eV for Fe, 6539.0 eV for Mn). Scans were carried out over the energy ranges of 6880−7930 eV (Fe) and 6310−7110 eV (Mn) for 685 and 800 s durations, respectively. Sample temperature was maintained at 10 K in an Oxford liquid helium cryostat.

Data processing was performed using the EXAFSPAK software package.[85] Three-segment splines (of orders 2, 3, and 3) were removed from the EXAFS using PySpline[86] and the EXAFS data were then fit using OPT. Scattering paths for EXAFS fits were generated from appropriate structural models using FEFF 9.0 (additional details can be found in the Supporting Information).[87]

XAS Damage Assessment. Due to the presence of two different high-valent metal ions in **4**/**4**, care was required to ensure that both metals remained stable during both Fe and Mn scans. Initially, fresh sample spots and highly attenuated beam were used to collect rapid edge scans (60−100 s exposure) for both Fe and Mn; given the short exposure time and low incident intensity, these spectra were taken to be undamaged. Then, to assess the stability of a metal during its own scan (e.g., Fe), a new spot was used to collect a full EXAFS scan at the Fe edge, followed on the same spot by a rapid Fe edge scan; only when the rapid edge scan overlaid with the initial, undamaged edge spectrum was the EXAFS scan deemed to have a safe level of exposure. This process was then repeated on a new sample spot, except that, instead of rescanning the Fe edge afterward, a rapid Mn edge scan was collected and compared to the undamaged Mn edge spectrum to ensure that the Mn was also stable during the Fe scan. When the Fe scan was established, this entire process was repeated for Mn. The process of performing a full EXAFS scan in order to assess damage was found to be critically important due to the energy dependence of the X-ray flux; simply performing repeated rapid edge scans until damage became apparent was found to overestimate safe exposure times by a significant margin (~10%). Edge overlays and additional details can be found in Figures S7 and S8.

EPR Measurements. X-band CW measurements were performed on a Bruker ESP 300 spectrometer with an ER 041 MR microwave bridge and an ER 4116DM resonator. All other EPR measurements were performed on a Bruker Elexsys E580 X-band spectrometer equipped with a SuperX-FT microwave bridge. For pulse EPR measurements at X-band, a Bruker EN 4118X-MD4 dielectric ENDOR resonator was used in concert with an Oxford CF935 helium flow cryostat. Pulse EPR spectra at Q-band frequencies were acquired using a home-built intermediate-frequency extension of the SuperX-FT X-band bridge equipped with a Millitech 5W pulse power amplifier.

EPR Analysis. Data processing and spectral simulations were performed using Kazan viewer, a home-written suite of utilities in MATLAB.[88] One-dimensional EPR simulations were performed using the "pepper" utility from the EasySpin software package.[89] ENDOR data were analyzed by simultaneous frequency domain simulation of all field-dependent spectra until a satisfactory solution was achieved. Euler angles are reported with respect to the ^{55}Mn hyperfine coupling tensor, which is colinear with the *g* matrix in our simulations.

ASSOCIATED CONTENT

Supporting Information

The Supporting Information is available free of charge on the ACS Publications website at DOI: 10.1021/jacs.6b11563.

Additional details concerning sample preparation, data collection, and analysis; additional EPR spectra; Mössbauer analysis of sample composition; X-ray damage assessment; X-ray analysis of Fe-only and Mn-only control samples; tables of EXAFS fits (PDF)

AUTHOR INFORMATION

Corresponding Authors

*aus40@psu.edu
*cjp27@psu.edu

ORCID

Carsten Krebs: 0000-0002-3302-7053
Christopher J. Pollock: 0000-0001-5736-513X

Notes

The authors declare no competing financial interest.

ACKNOWLEDGMENTS

This material is based upon work supported by the National Science Foundation Graduate Research Fellowship Program under Grant No. DGE1255832. C.J.P. and E.J.B. thank the NIH for National Research Service Awards (GM113389-01 and GM116353-01). This work was supported by the National Institutes of Health (GM55365 to J.M.B. and C.K.). Portions of this work were conducted at the Stanford Synchrotron Radiation Lightsource, SLAC National Accelerator Laboratory, which is supported by the U.S. Department of Energy, Office of Science, Office of Basic Energy Sciences under Contract No. DE-AC02-76SF00515. The SSRL Structural Molecular Biology Program is supported by the DOE Office of Biological and Environmental Research, and by the National Institutes of Health, National Institute of General Medical Sciences (including P41GM103393).

REFERENCES

(1) Krebs, C.; Galonić Fujimori, D.; Walsh, C. T.; Bollinger, J. M., Jr. *Acc. Chem. Res.* **2007**, *40*, 484−492.
(2) Price, J. C.; Barr, E. W.; Tirupati, B.; Bollinger, J. M., Jr.; Krebs, C. *Biochemistry* **2003**, *42*, 7497−7508.
(3) Hoffart, L. M.; Barr, E. W.; Guyer, R. B.; Bollinger, J. M., Jr.; Krebs, C. *Proc. Natl. Acad. Sci. U. S. A.* **2006**, *103*, 14738−14743.
(4) Galonić, D. P.; Barr, E. W.; Walsh, C. T.; Bollinger, J. M., Jr.; Krebs, C. *Nat. Chem. Biol.* **2007**, *3*, 113−116.

DOI: 10.1021/jacs.6b11563
J. Am. Chem. Soc. 2017, 139, 1950−1957

(5) Wang, C.; Chang, W.-c.; Guo, Y.; Huang, H.; Peck, S. C.; Pandelia, M.-E.; Lin, G.; Liu, H.; Krebs, C.; Bollinger, J. M., Jr. *Science* **2013**, *342*, 991−995.
(6) Chang, W.-c.; Guo, Y.; Wang, C.; Butch, S. E.; Rosenzweig, A. C.; Boal, A. K.; Krebs, C.; Bollinger, J. M., Jr. *Science* **2014**, *343*, 1140−1144.
(7) Bollinger, J. M., Jr.; Chang, W.-c.; Matthews, M. L.; Martinie, R. J.; Boal, A. K.; Krebs, C. In *2-Oxoglutarate-Dependent Oxygenases*; Hausinger, R. P., Schofield, C. J., Eds.; Royal Society of Chemistry: London, 2015.
(8) Kovaleva, E. G.; Neibergall, M. B.; Chakrabarty, S.; Lipscomb, J. D. *Acc. Chem. Res.* **2007**, *40*, 475−483.
(9) Lee, S. K.; Fox, B. G.; Froland, W. A.; Lipscomb, J. D.; Münck, E. *J. Am. Chem. Soc.* **1993**, *115*, 6450−6451.
(10) Shu, L.; Nesheim, J. C.; Kauffmann, K.; Münck, E.; Lipscomb, J. D.; Que, L., Jr. *Science* **1997**, *275*, 515−518.
(11) Banerjee, R.; Proshlyakov, Y.; Lipscomb, J. D.; Proshlyakov, D. A. *Nature* **2015**, *518*, 431−434.
(12) Sturgeon, B. E.; Burdi, D.; Chen, S.; Huynh, B. H.; Edmondson, D. E.; Stubbe, J.; Hoffman, B. M. *J. Am. Chem. Soc.* **1996**, *118*, 7551−7557.
(13) Stubbe, J.; van der Donk, W. A. *Chem. Rev.* **1998**, *98*, 705−762.
(14) Jiang, W.; Yun, D.; Saleh, L.; Barr, E. W.; Xing, G.; Hoffart, L. M.; Maslak, M.-A.; Krebs, C.; Bollinger, J. M., Jr. *Science* **2007**, *316*, 1188−1191.
(15) Cotruvo, J. A., Jr.; Stich, T. A.; Britt, R. D.; Stubbe, J. *J. Am. Chem. Soc.* **2013**, *135*, 4027−4039.
(16) Umena, Y.; Kawakami, K.; Shen, J.-R.; Kamiya, N. *Nature* **2011**, *473*, 55−60.
(17) Cox, N.; Pantazis, D. A.; Neese, F.; Lubitz, W. *Acc. Chem. Res.* **2013**, *46*, 1588−1596.
(18) Cox, N.; Retegan, M.; Neese, F.; Pantazis, D. A.; Boussac, A.; Lubitz, W. *Science* **2014**, *345*, 804−808.
(19) Rittle, J.; Green, M. T. *Science* **2010**, *330*, 933−937.
(20) Yosca, T. H.; Rittle, J.; Krest, C. M.; Onderko, E. L.; Silakov, A.; Calixto, J. C.; Behan, R. K.; Green, M. T. *Science* **2013**, *342*, 825−829.
(21) Bollinger, J. M., Jr.; Broderick, J. B. *Curr. Opin. Chem. Biol.* **2009**, *13*, 51−57.
(22) Krebs, C.; Bollinger, J. M., Jr.; Booker, S. J. *Curr. Opin. Chem. Biol.* **2011**, *15*, 291−303.
(23) Lee, S. K.; Nesheim, J. C.; Lipscomb, J. D. *J. Biol. Chem.* **1993**, *268*, 21569−21577.
(24) Fox, B. G.; Lyle, K. S.; Rogge, C. E. *Acc. Chem. Res.* **2004**, *37*, 421−429.
(25) Warui, D. M.; Li, N.; Nørgaard, H.; Krebs, C.; Bollinger, J. M., Jr.; Booker, S. J. *J. Am. Chem. Soc.* **2011**, *133*, 3316−3319.
(26) Li, N.; Nørgaard, H.; Warui, D. M.; Booker, S. J.; Krebs, C.; Bollinger, J. M., Jr. *J. Am. Chem. Soc.* **2011**, *133*, 6158−6161.
(27) Li, N.; Chang, W.-c.; Warui, D. M.; Booker, S. J.; Krebs, C.; Bollinger, J. M., Jr. *Biochemistry* **2012**, *51*, 7908−7916.
(28) Pandelia, M.-E.; Li, N.; Nørgaard, H.; Warui, D. M.; Rajakovich, L. J.; Chang, W.-c.; Booker, S. J.; Krebs, C.; Bollinger, J. M., Jr. *J. Am. Chem. Soc.* **2013**, *135*, 15801−15812.
(29) Rajakovich, L. J.; Nørgaard, H.; Warui, D. M.; Chang, W.-c.; Li, N.; Booker, S. J.; Krebs, C.; Bollinger, J. M., Jr.; Pandelia, M.-E. *J. Am. Chem. Soc.* **2015**, *137*, 11695−11709.
(30) Nordlund, P.; Reichard, P. *Annu. Rev. Biochem.* **2006**, *75*, 681−706.
(31) Stubbe, J.; Nocera, D. G.; Yee, C. S.; Chang, M. C. Y. *Chem. Rev.* **2003**, *103*, 2167−2202.
(32) Licht, S.; Gerfen, G. J.; Stubbe, J. *Science* **1996**, *271*, 477−481.
(33) Tomter, A. B.; Zoppellaro, G.; Andersen, N. H.; Hersleth, H.-P.; Hammerstad, M.; Røhr, Å. K.; Sandvik, G. K.; Strand, K. R.; Nilsson, G. E.; Bell, C. B., III; Barra, A.-L.; Blasco, E.; Le Pape, L.; Solomon, E. I.; Andersson, K. K. *Coord. Chem. Rev.* **2013**, *257*, 3−26.
(34) Bollinger, J. M., Jr.; Krebs, C.; Vicol, A.; Chen, S.; Ley, B. A.; Edmondson, D. E.; Huynh, B. H. *J. Am. Chem. Soc.* **1998**, *120*, 1094−1095.
(35) Moënne-Loccoz, P.; Baldwin, J.; Ley, B. A.; Loehr, T. M.; Bollinger, J. M., Jr. *Biochemistry* **1998**, *37*, 14659−14663.
(36) Skulan, A. J.; Brunold, T. C.; Baldwin, J.; Saleh, L.; Bollinger, J. M., Jr.; Solomon, E. I. *J. Am. Chem. Soc.* **2004**, *126*, 8842−8855.
(37) Burdi, D.; Sturgeon, B. E.; Tong, W. H.; Stubbe, J.; Hoffman, B. M. *J. Am. Chem. Soc.* **1996**, *118*, 281−282.
(38) Ehrenberg, A.; Reichard, P. *J. Biol. Chem.* **1972**, *247*, 3485−3488.
(39) Atkin, C. L.; Thelander, L.; Reichard, P.; Lang, G. *J. Biol. Chem.* **1973**, *248*, 7464−7472.
(40) Sjöberg, B.-M.; Reichard, P. *J. Biol. Chem.* **1977**, *252*, 536−541.
(41) Sjöberg, B.-M.; Reichard, P.; Gräslund, A.; Ehrenberg, A. *J. Biol. Chem.* **1978**, *253*, 6863−6865.
(42) Larsson, A.; Sjöberg, B.-M. *EMBO J.* **1986**, *5*, 2037−2040.
(43) Cotruvo, J. A., Jr.; Stubbe, J. *Biochemistry* **2010**, *49*, 1297−1309.
(44) Cox, N.; Ogata, H.; Stolle, P.; Reijerse, E.; Auling, G.; Lubitz, W. *J. Am. Chem. Soc.* **2010**, *132*, 11197−11213.
(45) Cotruvo, J. A., Jr.; Stubbe, J. *Biochemistry* **2011**, *50*, 1672−1681.
(46) Boal, A. K.; Cotruvo, J. A., Jr.; Stubbe, J.; Rosenzweig, A. C. *Science* **2010**, *329*, 1526−1530.
(47) Högbom, M.; Stenmark, P.; Voevodskaya, N.; McClarty, G.; Gräslund, A.; Nordlund, P. *Science* **2004**, *305*, 245−248.
(48) Jiang, W.; Bollinger, J. M., Jr.; Krebs, C. *J. Am. Chem. Soc.* **2007**, *129*, 7504−7505.
(49) Voevodskaya, N.; Lendzian, F.; Ehrenberg, A.; Gräslund, A. *FEBS Lett.* **2007**, *581*, 3351−3355.
(50) Bollinger, J. M., Jr.; Jiang, W.; Green, M. T.; Krebs, C. *Curr. Opin. Struct. Biol.* **2008**, *18*, 650−657.
(51) Jiang, W.; Yun, D.; Saleh, L.; Bollinger, J. M., Jr.; Krebs, C. *Biochemistry* **2008**, *47*, 13736−13744.
(52) Jiang, W.; Hoffart, L. M.; Krebs, C.; Bollinger, J. M., Jr. *Biochemistry* **2007**, *46*, 8709−8716.
(53) Jiang, W.; Saleh, L.; Barr, E. W.; Xie, J.; Gardner, M. M.; Krebs, C.; Bollinger, J. M., Jr. *Biochemistry* **2008**, *47*, 8477−8484.
(54) Younker, J. M.; Krest, C. M.; Jiang, W.; Krebs, C.; Bollinger, J. M., Jr.; Green, M. T. *J. Am. Chem. Soc.* **2008**, *130*, 15022−15027.
(55) Xue, G.; Wang, D.; De Hont, R.; Fiedler, A. T.; Shan, X.; Münck, E.; Que, L., Jr. *Proc. Natl. Acad. Sci. U. S. A.* **2007**, *104*, 20713−20718.
(56) Rinaldo, D.; Philipp, D. M.; Lippard, S. J.; Friesner, R. A. *J. Am. Chem. Soc.* **2007**, *129*, 3135−3147.
(57) Han, W.-G.; Noodleman, L. *Inorg. Chim. Acta* **2008**, *361*, 973−986.
(58) Han, W.-G.; Giammona, D. A.; Bashford, D.; Noodleman, L. *Inorg. Chem.* **2010**, *49*, 7266−7281.
(59) Riggs-Gelasco, P. J.; Shu, L.; Chen, S.; Burdi, D.; Huynh, B. H.; Que, L., Jr.; Stubbe, J. *J. Am. Chem. Soc.* **1998**, *120*, 849−860.
(60) Dassama, L. M. K.; Silakov, A.; Krest, C. M.; Calixto, J. C.; Krebs, C.; Bollinger, J. M., Jr.; Green, M. T. *J. Am. Chem. Soc.* **2013**, *135*, 16758−16761.
(61) Mitić, N.; Saleh, L.; Schenk, G.; Bollinger, J. M., Jr.; Solomon, E. I. *J. Am. Chem. Soc.* **2003**, *125*, 11200−11201.
(62) Mitić, N.; Clay, M. D.; Saleh, L.; Bollinger, J. M., Jr.; Solomon, E. I. *J. Am. Chem. Soc.* **2007**, *129*, 9049−9065.
(63) Willems, J.-P.; Lee, H.-I.; Burdi, D.; Doan, P. E.; Stubbe, J.; Hoffman, B. M. *J. Am. Chem. Soc.* **1997**, *119*, 9816−9824.
(64) Burdi, D.; Willems, J.-P.; Riggs-Gelasco, P. J.; Antholine, W. E.; Stubbe, J.; Hoffman, B. M. *J. Am. Chem. Soc.* **1998**, *120*, 12910−12919.
(65) Shanmugam, M.; Doan, P. E.; Lees, N. S.; Stubbe, J.; Hoffman, B. M. *J. Am. Chem. Soc.* **2009**, *131*, 3370−3376.
(66) Doan, P. E.; Shanmugam, M.; Stubbe, J.; Hoffman, B. M. *J. Am. Chem. Soc.* **2015**, *137*, 15558−15566.
(67) Andersson, C. S.; Högbom, M. *Proc. Natl. Acad. Sci. U. S. A.* **2009**, *106*, 5633−5638.
(68) Shafaat, H. S.; Griese, J. J.; Pantazis, D. A.; Roos, K.; Andersson, C. S.; Popović-Bijelić, A.; Gräslund, A.; Siegbahn, P. E. M.; Neese, F.; Lubitz, W.; Högbom, M.; Cox, N. *J. Am. Chem. Soc.* **2014**, *136*, 13399−13409.

DOI: 10.1021/jacs.6b11563
J. Am. Chem. Soc. 2017, 139, 1950−1957

(69) Dassama, L. M. K.; Yosca, T. H.; Conner, D. A.; Lee, M. H.; Blanc, B.; Streit, B. R.; Green, M. T.; DuBois, J. L.; Krebs, C.; Bollinger, J. M., Jr. *Biochemistry* **2012**, *51*, 1607−1616.
(70) Beckwith, M. A.; Ames, W.; Vila, F. D.; Krewald, V.; Pantazis, D. A.; Mantel, C.; Pécaut, J.; Gennari, M.; Duboc, C.; Collomb, M.-N.; Yano, J.; Rehr, J. J.; Neese, F.; DeBeer, S. *J. Am. Chem. Soc.* **2015**, *137*, 12815−12834.
(71) Baldwin, M. J.; Stemmler, T. L.; Riggs-Gelasco, P. J.; Kirk, M. L.; Penner-Hahn, J. E.; Pecoraro, V. L. *J. Am. Chem. Soc.* **1994**, *116*, 11349−11356.
(72) Hsu, H.-F.; Dong, Y.; Shu, L.; Young, V. G., Jr.; Que, L., Jr. *J. Am. Chem. Soc.* **1999**, *121*, 5230−5237.
(73) Xue, G.; Fiedler, A. T.; Martinho, M.; Münck, E.; Que, L., Jr. *Proc. Natl. Acad. Sci. U. S. A.* **2008**, *105*, 20615−20620.
(74) Andersson, C. S.; Öhrström, M.; Popović-Bijelić, A.; Gräslund, A.; Stenmark, P.; Högbom, M. *J. Am. Chem. Soc.* **2012**, *134*, 123−125.
(75) Dassama, L. M. K.; Boal, A. K.; Krebs, C.; Rosenzweig, A. C.; Bollinger, J. M., Jr. *J. Am. Chem. Soc.* **2012**, *134*, 2520−2523.
(76) Dassama, L. M. K.; Krebs, C.; Bollinger, J. M., Jr.; Rosenzweig, A. C.; Boal, A. K. *Biochemistry* **2013**, *52*, 6424−6436.
(77) Larson, E.; Lah, M. S.; Li, X.; Bonadies, J. A.; Pecoraro, V. L. *Inorg. Chem.* **1992**, *31*, 373−378.
(78) Schäfer, K.-O.; Bittl, R.; Zweygart, W.; Lendzian, F.; Haselhorst, G.; Weyhermüller, T.; Wieghardt, K.; Lubitz, W. *J. Am. Chem. Soc.* **1998**, *120*, 13104−13120.
(79) Jensen, A. F.; Su, Z.; Hansen, N. K.; Larsen, F. K. *Inorg. Chem.* **1995**, *34*, 4244−4252.
(80) Wang, D.; Farquhar, E. R.; Stubna, A.; Münck, E.; Que, L., Jr. *Nat. Chem.* **2009**, *1*, 145−150.
(81) Kwak, Y.; Jiang, W.; Dassama, L. M. K.; Park, K.; Bell, C. B., III.; Liu, L. V.; Wong, S. D.; Saito, M.; Kobayashi, Y.; Kitao, S.; Seto, M.; Yoda, Y.; Alp, E. E.; Zhao, J.; Bollinger, J. M., Jr.; Krebs, C.; Solomon, E. I. *J. Am. Chem. Soc.* **2013**, *135*, 17573−17584.
(82) Thomann, H.; Bernardo, M.; McCormick, J. M.; Pulver, S.; Andersson, K. K.; Lipscomb, J. D.; Solomon, E. I. *J. Am. Chem. Soc.* **1993**, *115*, 8881−8882.
(83) DeRose, V. J.; Liu, K. E.; Lippard, S. J.; Hoffman, B. M. *J. Am. Chem. Soc.* **1996**, *118*, 121−134.
(84) DeRose, V. J.; Liu, K. E.; Kurtz, D. M., Jr.; Hoffman, B. M.; Lippard, S. J. *J. Am. Chem. Soc.* **1993**, *115*, 6440−6441.
(85) George, G. N. *EXAFSPAK*, EXAFSPAK, SSRL, SLAC; Stanford University: Stanford, CA.
(86) Tenderholt, A.; Hedman, B.; Hodgson, K. O. *AIP Conf. Proc.* **2006**, *882*, 105−107.
(87) Rehr, J. J.; Kas, J. J.; Vila, F. D.; Prange, M. P.; Jorissen, K. *Phys. Chem. Chem. Phys.* **2010**, *12*, 5503−5513.
(88) Kazan Viewer - Homepage Alexey Silakov, https://sites.google.com/site/silakovalexey/kazan-viewer (accessed October 14, 2016).
(89) Stoll, S.; Schweiger, A. *J. Magn. Reson.* **2006**, *178*, 42−55.

DOI: 10.1021/jacs.6b11563
J. Am. Chem. Soc. 2017, 139, 1950−1957